Advanced active polymer probe for near-field optics

Hongshi Chen, Quanbo Jiang, Ali Issa, Borui Li, Dandan Ge, Safi Jradi, Jacques Lalevee, Sylvie Marguet, Regis Deturche, Christophe Couteau, et al.

Optics Letters

Advanced active polymer probe for near-field optics

Hongshi Chen,[1] Quanbo Jiang,[1,*] Ali Issa,[1] Borui Li,[1] Dandan Ge,[1] Safi Jradi,[1] Jacques Lalevee,[2] Sylvie Marguet,[3] Regis Deturche,[1] Christophe Couteau,[1] Jerome Plain,[1] and Renaud Bachelot[1]

[1]Light, Nanomaterials, Nanotechnologies (L2n) Laboratory, CNRS EMR 7004, University of Technology of Troyes, 12 rue Marie Curie, 10004 Troyes, France
[2]Institut de Science des Matériaux de Mulhouse IS2M, UMR CNRS 7361, ENSCMu-UHA, 68057, France
[3]Université Paris-Saclay, CEA, CNRS, NIMBE, 91190 Gif-sur-Yvette, France
*quanbo.jiang@utt.fr

Received 22 May 2023; accepted 10 July 2023; posted 17 July 2023; published 1 August 2023

We report on a novel, to the best of our knowledge, active probe for scanning near-field optical microscopy (SNOM). A fluorescent nanosphere, acting as the secondary source, is grafted in an electrostatic manner at the apex of a polymer tip integrated into the extremity of an optical fiber. Thanks to the high photostability and sensitivity of the secondary source, the near-field interaction with a gold nanocube is investigated. It is shown that the spatial resolution is well defined by the size of the fluorescent nanosphere. The polarization-dependent near-field images, which are consistent with the simulation, are ascribed to the local excitation rate enhancement. Meanwhile, measurement of the distance-dependent fluorescence lifetime of the nanosphere provides strong evidence that the local density of states is modified so that extra information on nano-emitters can be extracted during near-field scanning. This advanced active probe can thus potentially broaden the range of applications to include nanoscale thermal imaging, biochemical sensors, and the manipulation of nanoparticles.

https://doi.org/10.1364/OL.495861

Scanning near-field optical microscopy (SNOM), a technology for high-spatial-resolution optical imaging, allows the acquisition of near-field information beyond the diffraction limit [1]. The probe tip as the key factor for determining the quality of measurements has been widely developed using both aperture or aperture-less probes [2,3]. Furthermore, the use of an active probe consisting of a nanoemitter acting as a secondary source at the apex of an optical fiber tip improves the spatial resolution by filtering the scattering incident light from the classical probe tip and avoiding the thermal effect from metal coating layers [4]. Nanoemitters such as fluorescent nanospheres [5], nanodiamonds [6], and nanocrystals [7] have been used for realizing active probes. However, during the anchoring and scanning steps, the unreliability of the secondary source, including the physical contact with the tip as well as the photostability, limits its potential applications [8]. Herein, we develop a novel active probe by grafting a fluorescent nanosphere at the apex of a polymer tip that can act as a microlens [9,10] with the aim of overcoming the lack of stability of the secondary source. Taking advantage of the high intensity of the fluorescent nanosphere and its high sensitivity to the near-field radiation, this active probe enables the range of applications of near-field scanning techniques to be broadened to the nanoscale characterizations of optical properties such as plasmonic hot spots, the photoluminescence properties of gold nanostructures, and optical polarization responses [11,12].

In this Letter, we report on the use of an original optical active nanoprobe and illustrate its interest through its near-field interaction with a gold nanocube. The probe shown in Fig. 1(a) consists of a functionalized polymer tip integrated by photopolymerization at the apex of a single-mode optical fiber [9] and a 50 nm (or 200 nm) fluorescent nanosphere (FluoSpheres F8770/F8810; Invitrogen, surface modified with carboxylate) which is attached at the extremity of the tip by an electrostatic interaction and acts as the secondary source [13]. The fabrication procedure for this active probe is given in Sections 1 and 2 of Supplement 1. Figure 1(b) shows the experimental setup for near-field studies. The fiber-based active probe is glued onto one arm of the tuning fork, while the probe–sample distance is controlled by a shear-force method [14]. A pulsed 532 nm excitation laser beam, whose energy lies in the absorption spectrum of the fluorescence nanosphere [see Fig. 1(c)], is aligned with the active probe through an oil immersion objective (Olympus, 100×, 1.4 NA) from the bottom of the sample stage. The backreflected light is then collected through the same objective before coupling via an objective lens (Olympus, 4×, 0.17 NA) into an optical fiber with a 50 μm core diameter which is connected to an avalanche photodiode (APD, SPCM-AQRH-15-FC) detector. The fiber core acts as a pinhole in the confocal system. In addition, a 570 nm long-pass filter is inserted into the path of detection to eliminate the excitation wavelength and accordingly to obtain the red fluorescent signal of the nanosphere at around 608 nm, as indicated in Fig. 1(c). While the sample stage is scanning, as illustrated in Fig. 1(d), a point-to-point sample image from the reflected light is acquired. We emphasize that both the incident laser spot and the position of the active probe are aligned and fixed while the sample surface is scanned. Since the nanosphere is attached slightly asymmetrically, as observed from the SEM images in Fig. 1(a), the near-field images of symmetric objects like a nanocube here

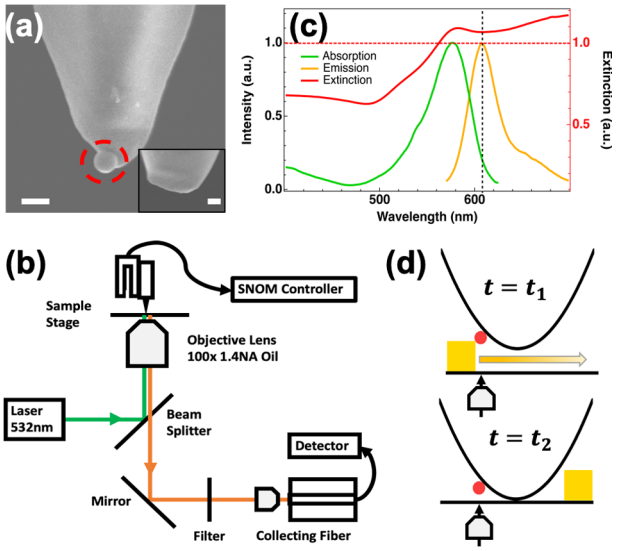

Fig. 1. (a) SEM images of the active polymer probes with scale bars of 300 nm. The dashed circle highlights the position of a 200 nm nanosphere. The inset displays the probe with a 50 nm nanosphere. (b) Schematic of the scanning near-field optical microscopy (SNOM) system. (c) Absorption and emission spectra of the solution of nanospheres as well as the extinction spectrum of the nanocube colloid solution. (d) Sketches showing sample scanning from the right to the left edge of a nanocube. The active probe (indicated by a black curve with a red dot) and the objective are both kept immobilized during scanning (see Visualization 1).

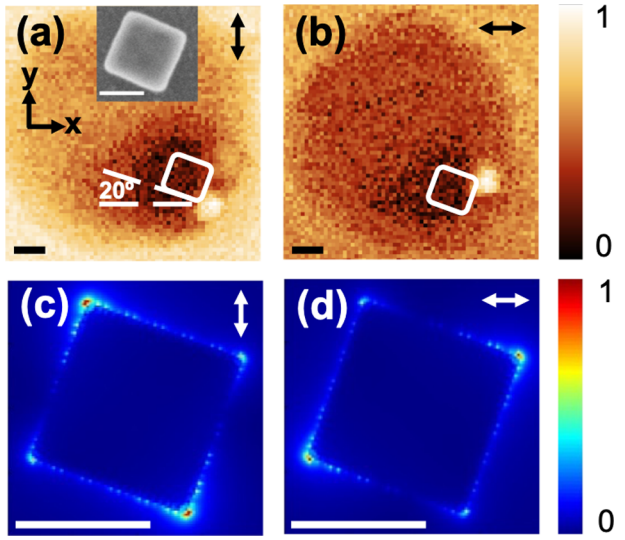

Fig. 2. (a), (b) Fluorescence scanning near-field images of the nanocube with indicated polarizations of the excited laser beam. The inset shows an SEM image of this nanocube. The scale bars are 100 nm. (c), (d) FDTD simulation of optical near-field images (at 532 nm) of the nanocube with corresponding incident polarizations and a color bar normalized to the maximum intensity. The scale bars are 100 nm.

will highly depend on the relative position of this secondary source.

The sample investigated here is an individual gold nanocube deposited on the glass cover slip by evaporating a drop of a nanocube colloid solution with a relatively low concentration [its extinction spectrum is shown in in Fig. 1(c)]. The preselected nanocube is measured to have side lengths of 130 nm and a 20° tilt compared to the x axis, as shown in Fig. 2(a). When the active probe with a 50 nm nanosphere gets close to the corner of the nanocube in the constant distance mode, the fluorescence of the nanosphere is highly enhanced, so the near-field information can be steadily detected [15]. The central dark areas in Figs. 2(a) and 2(b) can be attributed to the lack of excitation light, which is blocked by the nanocube, and thus indicate the contour of the nanocube. Thanks to the asymmetric location of the nanosphere, the bright spots in the fluorescence images are always located on the right edge of the nanocube under linear polarization along the x and y axes.

More specifically, the nearest distance between the nanosphere and the nanocube occurs when the right edge of the nanocube is moving toward the active probe, as illustrated in Fig. 1(d) at time t_1. The huge electric field enhancement at the corner of the nanocube results in a strong fluorescence signal through the enhancement of the local excitation field at 532 nm as well as the nanosphere emission because the extinction spectrum of the nanocube is higher than 1 when it overlaps with both the absorption and the emission spectra of the nanosphere, as indicated in Fig. 1(c). When the probe is raised to scan the whole nanocube, the fluorescence of the nanosphere is not visible because the nanocube blocks the excitation laser, which is why a dark contrast comes after the bright spot. Since the nanosphere is attached slightly on the left of the apex of the polymer tip, the distance between the nanosphere and the left edge of the nanocube at time t_2 [Fig. 1(d)] is greater than that at time t_1; that's the reason why we do not observe a second bright spot at the corner of the left edge. Eventually, the fluorescence signal gradually becomes brighter because the nanosphere starts to move close to the surface without the nanocube. More details about the scanning of this nanocube are shown in Section 3 of Supplement 1.

In addition, we observe that the right border of the dark area shows a clearer edge profile than other sides, which means that the nanocube and the nanosphere are at their closest, leading to better resolution. It turns out again that when the scanning direction is from the right to the left edge, only the near-field hotspot comes out at the right edge of the nanocube, while the nanosphere cannot reach the near field of the nanocube for the other edges of the nanocube. In Figs. 2(a) and 2(b), we also observe that when the direction of the incident linear polarization is varied from the y direction to the x direction, the bright spot moves from the lower part to the upper part. The shift of this bright spot is measured to be 150±6 nm in the fluorescent image, which roughly corresponds to the side length of the nanocube. It turns out that the near-field fluorescence image obtained using the active probe provides not only spatial sensitivity but also polarization sensitivity. The FDTD simulation results (FDTD Solutions by Ansys Lumerical) displayed in Figs. 2(c) and 2(d) elaborate on the optical near-field electric field intensity distribution of the nanocube excited by a 532 nm plane wave. Considering the amplified field intensity at the same position of the nanocube, the simulation results are consistent with the experimental results where the bright spots are located in the corners of the nanocube, which highly depend on the polarization. In other words, the fluorescence bright spots result from the local enhancement of the rate of excitation due to electromagnetic hotspots at the nanocube corners at $\lambda = 532$ nm.

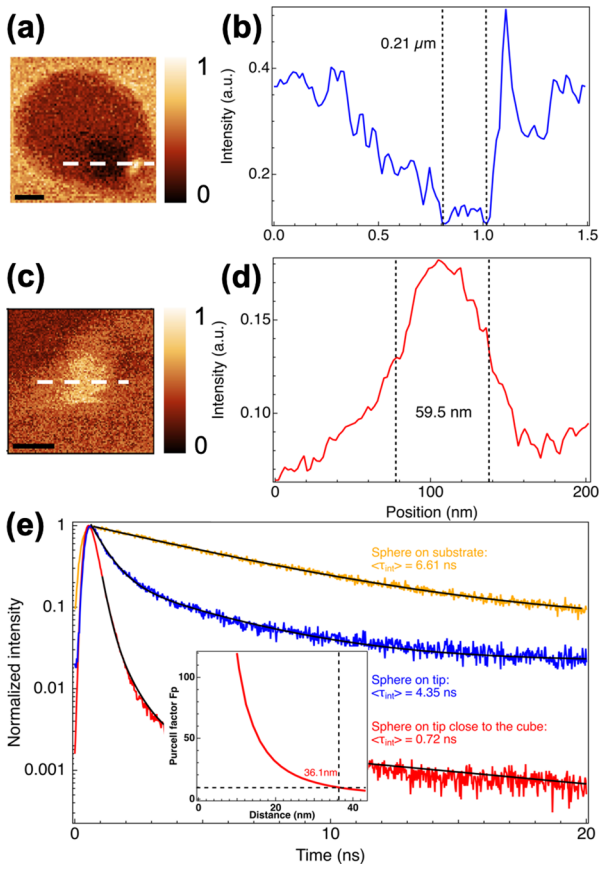

Fig. 3. (a), (c) Fluorescence near-field images of the nanocube with a fixed polarization. (c) Enlarged scanning image at the focus of the bright spot. The scale bars are 200 and 50 nm, respectively. (b), (d) Cross-section profiles along the dashed lines in (a) and (c), respectively. (e) Fluorescence lifetime decays of the nanosphere emission in different situations and intensity-averaged lifetimes determined from the numerical fits. The inset displays the Purcell factor as function of the distance between the nanosphere and the nanocube according to the numerical simulation.

We further investigate the cross-section profiles of the fluorescence near-field images in Figs. 3(a) and 3(c) with the aim of assessing the spatial resolution. According to the profile shown in Fig. 3(b), which corresponds to the dashed line across the dark zone and the bright spot, the distance between the two lowest intensities is measured to be 210±22 nm, which is in the range of the diagonal of the nanocube (183 nm). It turns out that the shadowed area corresponds well to the nanocube with a small tilt with respect to the x axis of the image. Thanks to a zoomed-in scanning image of the bright spot in Fig. 3(a), the full width at half maximum of this bright spot in the profile of Fig. 3(d) can be estimated as 59.5±6.9 nm, which corresponds well to the supposed size of the nanosphere attached to the probe (50 nm). In other words, the spatial resolution corresponds to the size of the secondary fluorescent source, which could be further reduced. Taking advantage of the active probe scanning system, we are able to acquire extra information: the distance-dependent fluorescence lifetime of the nanosphere. Lifetime measurement was implemented using the time-correlated single photon counting (TCSPC) method. In Fig. 3(e), we report three cases: i) the nanosphere is on the glass substrate; ii) the nanosphere is attached to the polymer tip, which is landed on the substrate via shear force regulation; iii) the attached nanosphere is landed on the gold nanocube via shear force regulation. The intensity-averaged lifetimes indicated in Fig. 3(e) reveal a significant reduction when the surrounding changes.

Specifically, the lifetime of the nanosphere deposited on the glass substrate serves as a reference value: it is measured to be 6.61 ns. Once the nanosphere is attached to the polymer tip and landed on the glass substrate, the lifetime reduces to 4.35 ns due to the increase in the surrounding refractive index caused by the presence of the polymer probe [16]. When the nanosphere scans next to the nanocube corner, a significant decrease in the lifetime is observed: it drops to 0.72 ns, which is the signature of the Purcell effect close to a metal nanostructure [17] (the gold nanocube has a rich local density of states that act as efficient channel for deexciting the molecules within the spheres). Assuming that the nanosphere is only an effective point emitter located at the center of gravity, the experimental Purcell factor (F_p) is determined by knowing the lifetime reduction, which is the ratio between the lifetime of the nanosphere on the tip without the presence of the nanocube ($\tau^1 = 4.35$ ns) and the one measured near the nanocube ($\tau = 0.72$ ns) according to the following equation:

$$F_p = \frac{1}{q^1}\left(\frac{\tau^1}{\tau} - 1\right) + 1.$$

The factor q^1, which is the quantum yield of the nanosphere grafted onto the tip without the presence of the nanocube is determined as 0.58. The experimental Purcell factor is thus estimated to be 9.7. According to the FDTD numerical simulation, the Purcell factor is able to be deduced as a function of the distance between the point emitter and the gold nanocube [see the inset in Fig. 3(e)]. The distance between the center of the nanosphere and the nanocube corner is then determined as 36.1 ± 2.7 nm by applying the experimental Purcell factor to the curve. More details on lifetime fitting parameters and the theory of Purcell factor estimation are provided in Section 4 of Supplement 1. Thus, the sensitivity of our active probe to the fluorescence lifetime provides us with a new degree of freedom to study the emitter–gold nanocube energy transfer and to assess the distances between the probe and nano-objects [18].

In summary, we have reported a novel active probe with a fluorescent nanosphere grafted onto the apex of a polymer tip that is integrated onto an optical fiber. The stability of this secondary source allows the acquisition of a high-resolution fluorescence image resulting from the local interactions between the nanosphere and nano-objects without any degradation of the emission intensity after a long scanning time. The fluorescence scanning near-field image of the nanocube profile shows a strong polarization dependence along with a high spatial resolution limited by the size of the nanosphere. In addition, it is possible to thoroughly investigate the light–matter interaction between the secondary source and plasmonic nanostructures through fluorescence lifetime measurement. The lifetime reduction due to the Purcell effect could enable the study of couplings and associated distances between the nanoemitter and nanostructures at the nanoscale, which increases the potential to create tunable plasmonic nanostructures [19]. Altogether, considering its high sensitivity as well as its robust photostability, this advanced active probe could be used for many intriguing applications, such as nanoscale thermal imaging and spectroscopy, chemical or biochemical sensors, and the manipulation of nanoparticles [20,21].

Funding. China Scholarship Council; Agence Nationale de la Recherche (ANR-18-EURE-0013).

Acknowledgment. This work has benefited from the Nano'mat platform and was done within the framework of the Graduate School NANO-PHOT (Ecole Universitaire de Recherche, grant ANR-18-EURE-0013, CSC).

Disclosures. The authors declare that they have no conflict of interest.

Data availability. Data underlying the results presented in this paper are not publicly available at this time but may be obtained from the authors upon reasonable request.

Supplemental document. See Supplement 1 for supporting content.

REFERENCES

1. R. Bachelot, G. Lerondel, S. Blaize, S. Aubert, A. Bruyant, and P. Royer, Microsc. Res. Tech. **64**, 441 (2004).
2. N. Chevalier, Y. Sonnefraud, J. F. Motte, S. Huant, and K. Karrai, Rev. Sci. Instrum. **77**, 063704 (2006).
3. L. Billot, L. Berguiga, M. L. de la Chapelle, Y. Gilbert, and R. Bachelot, Eur. Phys. J. Appl. Phys. **31**, 139 (2005).
4. H. Wang, L. Wang, and X. G. Xu, Nat. Commun. **7**, 13212 (2016).
5. A. Cuche, B. Masenelli, G. Ledoux, D. Amans, C. Dujardin, Y. Sonnefraud, P. Mélinon, and S. Huant, Nanotechnology **20**, 015603 (2009).
6. A. Cuche, A. Drezet, Y. Sonnefraud, O. Faklaris, F. Treussart, J.-F. Roch, and S. Huant, Opt. Express **17**, 19969 (2009).
7. R. Jazi, T. P. L. Ung, P. Maso, G. C. D. Francs, M. Nasilowski, B. Dubertret, J.-P. Hermier, X. Quélin, and S. Buil, Phys. Chem. Chem. Phys. **20**, 16444 (2018).
8. I. Berline, C. Fiorini-Debuisschert, C. Royal, L. Douillard, and F. Charra, J. Appl. Phys. **104**, 103113 (2008).
9. R. Bachelot, C. Ecoffet, D. Deloeil, P. Royer, and D.-J. Lougnot, Appl. Opt. **40**, 5860 (2001).
10. R. Bachelot, S. Blaize, C. Pang, A. Bruyant, and P. Royer, Fiber Integr. Opt. **27**, 542 (2008).
11. P. Hsia, L. Douillard, F. Charra, S. Marguet, S. Kochtcheev, R. Bachelot, and C. Fiorini-Debuisschert, Proc. SPIE **9547**, 95470F (2015).
12. S. Hasegawa and K. Imura, J. Phys. Chem. C **126**, 5944 (2022).
13. A. Issa, I. Izquierdo, M. Merheb, D. Ge, A. Broussier, N. Ghabri, S. Marguet, C. Couteau, R. Bachelot, and S. Jradi, ACS Appl. Mater. Interfaces **13**, 41846 (2021).
14. K. Karrai and I. Tiemann, Phys. Rev. B **62**, 13174 (2000).
15. D. Ge, S. Marguet, and A. Issa, *et al.*, Nat. Commun. **11**, 3414 (2020).
16. A. Pillonnet, P. Fleury, A. I. Chizhik, A. M. Chizhik, D. Amans, G. Ledoux, F. Kulzer, A. J. Meixner, and C. Dujardin, Opt. Express **20**, 3200 (2012).
17. G. M. Akselrod, C. Argyropoulos, T. B. Hoang, C. Ciracì, C. Fang, J. Huang, D. R. Smith, and M. H. Mikkelsen, Nat. Photonics **8**, 835 (2014).
18. D. Ge, A. Issa, S. Jradi, C. Couteau, S. Marguet, and R. Bachelot, Photonics Res. **10**, 1552 (2022).
19. O. A. Yeshchenko, V. V. Kozachenko, A. V. Tomchuk, M. Haftel, R. J. Knize, and A. O. Pinchuk, J. Phys. Chem. C **123**, 13057 (2019).
20. J. S. Paiva, P. A. S. Jorge, C. C. Rosa, and J. P. S. Cunha, Biochim. Biophys. Acta, Gen. Subj. **1862**, 1209 (2018).
21. Y. Xiong and F. Xu, Adv. Photonics **2**, 064001 (2020).